Allosteric Effect of Amphiphile Binding to Phospholipase A_2[‡]

Bao-Zhu Yu,[§] Shi Bai,[§] Otto G. Berg,*[,||] and Mahendra K. Jain*[,§]

Department of Chemistry and Biochemistry, University of Delaware, Newark, Delaware 19716, and Department of Molecular Evolution, Uppsala University Evolutionary Biology Center, Uppsala, Sweden

Received July 2, 2008; Revised Manuscript Received December 30, 2008

ABSTRACT: In the preceding paper, we showed that the formation of the second premicellar complex of pig pancreatic IB phospholipase A2 (PLA2) can be considered a proxy for interface-activated substrate binding. Here we show that this conclusion is supported by results from premicellar $E_i^{\#}$ ($i = 1$, 2, or 3) complexes with a wide range of mutants of PLA2. Results also show a structural basis for the correlated functional changes during the formation of $E_2^{\#}$, and this is interpreted as an allosteric T (inactive) to R (active) transition. For example, the dissociation constant $K_2^{\#}$ for decylsulfate bound to $E_2^{\#}$ is lower at lower pH, at higher calcium concentrations, or with an inhibitor bound to the active site. Also, the lower limits of the $K_2^{\#}$ values are comparable under these conditions. The pH-dependent increase in $K_2^{\#}$ with a pK_a of 6.5 is attributed to E71 which participates in the binding of the second calcium which in turn influences the enzyme binding to phosphatidylcholine interface. Most mutants exhibited kinetic and spectroscopic behavior that is comparable to that of native PLA2 and ΔPLA2 with a deleted 62−66 loop. However, the ΔY52L substitution mutant cannot undergo the calcium-, pH-, or interface-dependent changes. We suggest that the Y52L substitution impairs the R to T transition and also hinders the approach of the Michaelis complex to the transition state. This allosteric change may be mediated by the structural motifs that connect the D48-D99 catalytic diad, the substrate-binding slot, and the residues of the i-face. Our interpretation is that the 57−72 loop and the $H_{48}DNCY_{52}$ segment of PLA2 are involved in transmitting the effect of the cooperative amphiphile binding to the i-face as a structural change in the active site.

Premicellar $E_i^{\#}$ ($i = 1$, 2, or 3) complexes of pig pancreatic IB phospholipase A_2 (PLA2)[1] are viable surrogates for some of the structural and functional states of the interface-activated E* form (*1*−*5*). $E_i^{\#}$ complexes have stoichiometry of N_i amphiphiles bound per enzyme with Hill numbers n_i and dissociation constant $K_i^{\#}$. These parameters provide a measure of multiple amphiphile interactions with the i-face. As shown in the preceding paper (*5*), the affinity of the inhibitor for $E_i^{\#}$ complexes is greater than that for the E form. It is analogous to the K_S* activation (*6, 7*) at the interface. Results in this paper show that the structural effects on the enzyme are responsible for an allosteric change by which a conformation change associated with the binding of amphiphiles to form $E_2^{\#}$ is correlated with enhanced inhibitor binding to the active site and, conversely, binding at the active site promotes a conformation with enhanced amphiphile binding to the interface.

Verheij and co-workers designed and characterized functional properties of a wide range of PLA2 mutants (*8*−*16*). These and other results (*1, 16*−*20*) are consistent with the key requirement of the interfacial kinetic paradigm for PLA2 (*21*) that the active site be buried inside the structure and that the i-face be on the surface of PLA2. These results also suggest coupling between the i-face and active site events mediated by the structural features of PLA2, including the 57−71 loop and the highly conserved H-bonding network (Figure 1). We characterize the premicellar complexes of the PLA2 mutants designed by Verheij et al. The key result is that decylsulfate binding to the i-face of $E_2^{\#}$ is enhanced in most mutants to the same limiting value at low pH, at high calcium concentrations, or with an inhibitor bound to the active site. These effects on $K_2^{\#}$ are not observed with the ΔY52L mutant with the Y52L substitution in the 62−66 loop deleted PLA2, and the results show that it remains frozen in one form. In the Appendix, the structural coupling between the i-face and active site is modeled in terms of an allosteric T (inactive) to R (active) transition, where the R state is the form that binds well at both the i-face and the active site. The results suggest that the Y52L substitution in ΔPLA2 confers a conformation that is permanently locked in the R form.

EXPERIMENTAL PROCEDURES

The research group of the late B. Verheij (Utrecht, The Netherlands) provided the mutants and PCU for this study.

‡ This work is dedicated to Bert Verheij (January 20, 1944, to August 1, 1998) who shared thoughts on PLA2.

* To whom correspondence should be addressed. Telephone: (302) 831-2968. Fax: (302) 831-6335. E-mail: mkjain@udel.edu.

§ University of Delaware.

|| Uppsala University Evolutionary Biology Center.

[1] Abbreviations: CMC, critical micelle concentration; DC_7PC, 1,2-diheptanoylphosphatidylcholine; DMPM, dimyristoylphosphatidylmethanol; HDNS, *N*-dansyl-hexadecylphosphoethanolamine; HEPES, 4-(2-hydroxyethyl)-1-piperazineethanesulfonic acid; i-face, interface binding surface of PLA2; MJ33, 1-hexadecyl-3-(trifluoroethyl)-*rac*-glycero-2-phosphomethanol; PCU, 2-dodecanylaminohexanol-2-phosphocholine; PLA2, secreted type IB phospholipase A_2 from pig pancreas; ΔPLA2, 62−66 loop deleted PLA2; ΔY52L, ΔPLA2 with the Y52L substitution; RET, fluorescence resonance energy transfer; STD, saturation transfer difference proton NMR; TMA-DPH, trimethylammonium diphenylhexatriene.

10.1021/bi801245s CCC: $40.75
Published on Web 03/20/2009

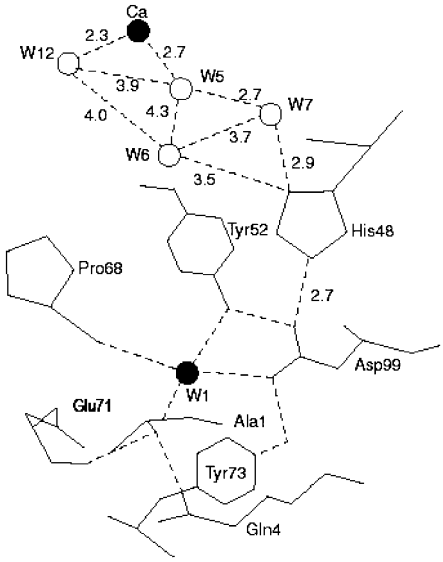

FIGURE 1: Hydrogen bonding network of PLA2 (*16, 32*) that consists of the structural water (W1), the NH_2 group of A1, the backbone oxygens of P68 and E71, the side chains of N4, Y52, and Y73, and the catalytic diad H48-D99(εNH). Calcium in the catalytic site is 7-coordinated to the carboxyl group of D49, backbone carbonyls of residues 28, 30, and 32, and two water molecules. The $H_{48}DNCY_{52}$ segment is localized on the 41−56 helix that links the 25−36 loop that binds the catalytic calcium and the 57−72 loop that binds the low-affinity calcium on the other side. Residues of these loops and the N- and C-terminal region provide side chains for the i-face interactions and allosteric coupling to the active site events via the H-bonding network.

Scheme 1

$$E \underset{n_1,K_1^{\#}}{\overset{+N_1\,A}{\rightleftharpoons}} E_1^{\#} \underset{n_2,K_2^{\#}}{\overset{+N_2\,A}{\rightleftharpoons}} E_2^{\#} \underset{n_3,K_3^{\#}}{\overset{+N_3\,A}{\rightleftharpoons}} E_3^{\#} \overset{+A^*}{\rightleftharpoons} E^*$$

Interfacial kinetic behavior of the mutants on DMPM (*22, 23*) vesicles or DC_7PC micelles (*7*) was characterized to ensure the integrity of the samples. The initial rates at 24 °C, pH 8.0, and a substrate mole fraction of 1 are given in the tables. The interfacial parameters expressed with an asterisk have the same meaning as those for the solution enzymes (*21, 24*). Other reagents, methods, protocols, and precautions used to characterize the binding of monodisperse amphiphiles to the i-face and the active site are as described previously (*1, 2, 17*).

Decylsulfate Binding to PLA2. Established experimental protocols, theory, and interpretation of the decylsulfate binding model in Scheme 1 are used (*1*−*3, 5, 17*) with specific details given below or in the figure captions and text. Typically, the decylsulfate concentration-dependent change in Trp-3 fluorescence from 1 or 2 μM PLA2 was monitored on an SLM-Aminco AB2 instrument. It was set in the ratio mode with 4 nm slit widths with excitation at 280 nm and emission at 333 nm for the Trp signal, or at 450 nm for the RET signal from the Trp/TMA-DPH pair, or at 490 nm from the Trp/HDNS pair. Intensity values obtained with an integration time of 4 s have a noise level of <1%. Controls with the W3F mutant of PLA2 showed that more than 97% of the reported signal intensity changes are from Trp-3. Also, the residual fluorescence from the tryosines does not change noticeably with the amphiphile binding to the i-face or the inhibitor binding to the active site. Measurements at pH 6.9 were taken in 10 mM HEPES, 10 mM Tris, 0.48 M NaCl, and 0.5 mM calcium or 1 mM EGTA with 1 mM EDTA. Buffers used for the pH dependence were acetate (pH 4−5), citrate (pH 5.5−6.5), HEPES (pH 6.5−7.5), Tris (pH 7.5−8.5), and borate (pH 9−10). The CMC of decylsulfate is 4.40 mM in the pH 6.9 buffer containing 0.48 M NaCl compared to a CMC of 4.50 in the absence of added NaCl (*17*).

Scheme 2

$$\begin{array}{ccccccc} E & \underset{n_1,K_1^{\#}}{\rightleftharpoons} & E_1^{\#} & \underset{n_2,K_2^{\#}}{\rightleftharpoons} & E_2^{\#} & \underset{n_3,K_3^{\#}}{\rightleftharpoons} & E_3^{\#} \\ \updownarrow K_I^{(0)} & & \updownarrow K_I^{(1)} & & \updownarrow K_I^{(2)} & & \updownarrow K_I^{(3)} \\ EI & \rightleftharpoons & E_1^{\#}I & \rightleftharpoons & E_2^{\#}I & \rightleftharpoons & E_3^{\#}I \end{array}$$

Decylsulfate titration curves were fitted as described below. The stepwise change in the Trp-3 emission intensity with the increasing concentration, c_f, of monodisperse decylsulfate below the CMC is analytically described as

$$\delta F = ((c_f/K_1^{\#})^{n_1}\{a_1 + (c_f/K_2^{\#})^{n_2}[a_2 + a_3(c_f/K_3^{\#})^{n_3}]\})/(1 + (c_f/K_1^{\#})^{n_1}\{1 + (c_f/K_2^{\#})^{n_2}[1 + (c_f/K_3^{\#})^{n_3}]\}) \quad (1)$$

Fit parameters for the decylsulfate titration curve (*2*) were obtained (Origin or MathCad) using the normalized intensity change δF ($=F/F_0 - 1$, where F_0 is the intensity of the E form and F is the intensity in the presence of decylsulfate). The intensity change parameter a_i for the $E_i^{\#}$ complex is relative to the E form. For example, an a_2 of +0.5 means that the emission intensity of $E_2^{\#}$ is 50% higher compared to that of E. An unresolved a_i does not necessarily rule out formation of other complexes whose Trp-3 signal may not be distinguishable.

All parameter estimates presented in this paper are based on using eq 1 to interpret the triphasic curves. In the presence of inhibitor, the estimated parameter values are apparent and can be considered as composites from the underlying physical events. Uncertainty in the reported fit parameters is <30% with a covariance of <0.90. We have not included the results where the uncertainty is likely to be >30%. Possible sources of run to run variability also include effects of the order of addition and slow drift in the Trp-3 fluorescence from the higher complexes presumably due to self-aggregation of premicellar complexes (*1*). When all such factors are taken into account, a >2-fold change in the reported $K_i^{\#}$ and n_i values is highly significant. We interpret and discuss only such changes.

Apparent Parameters. Unless mentioned otherwise, the calculated apparent $K_i^{\#}$ values (millimolar) were obtained at 5 μM PCU. As shown in the preceding paper (*5*), increasing amounts of PCU show clear shifts in the position of $E_2^{\#}$ formation. The simplest way to analyze these curves is to assume that binding of PCU at the active site influences the binding of decylsulfate at the i-face as modeled in Scheme 2 and derive the apparent i-face binding parameters at the different concentrations (I) of PCU. Horizontal steps are for the binding of decylsulfate to the i-face, and the upper row is the same as Scheme 1. The vertical steps correspond to binding of one PCU to the active site. The parameters for the horizontal steps in the second row are determined by the detailed balance conditions. The apparent parameters determined by application of the equations for Scheme 1, eq 1, are given by

$$K_i^{\#,\mathrm{app}} = K_i^{\#}\left(\frac{1 + I/K_I^{(i-1)}}{1 + I/K_I^{(i)}}\right)^{1/n_i}, \quad \text{for } i = 1, 2, \text{ or } 3 \quad (2)$$

$$A_i^{app} = \frac{A_i + A_i^{I} I/K_I^{(i)}}{1 + I/K_I^{(i)}}, \quad \text{for } i = 0, 1, 2, \text{ or } 3 \qquad (3a)$$

$$a_i^{app} = \frac{A_i^{app}}{A_0^{app}} - 1 \qquad (3b)$$

and $n_i^{app} = n_i$.

Scheme 2 and its interpretations are best applicable at the low concentration of PCU used for the results in this paper, where PCU is less likely to bind the i-face. Using eq 1 to analyze the results at 0, 2, 5, 7, and 15 μM PCU from the preceding paper (*5*) showed certain clear trends. For example, $K_1^{\#,app}$ is largely independent of PCU concentration, which shows (eq 2) that $K_1^{(1)} \approx K_1^{(0)}$ or that both are much greater than the inhibitor concentration. The strongest significant trend in these data is the decrease in $K_2^{\#,app}$ with an increase in PCU concentration, which is coupled to a simultaneous and significant decrease in A_2^{app}. In the context of this paper, both of these trends can be interpreted as a significant strengthening of the binding of PCU at the specific site in the $E_2^{\#}$ complex compared to both E and $E_1^{\#}$. In the Appendix, we consider a simplified variation of Scheme 2, where the coupling between $E_2^{\#}$ formation and active site binding derives from a conformational transition.

Saturation Transfer Difference (STD) NMR of Decylsulfate Bound to PLA2. As established in our laboratory (*3*), these measurements were taken on a Bruker 600 MHz spectrometer operating at 600.13 MHz under conditions given in the figure legend. Typically, a train of Gaussian-shaped RF saturation pulses (50 ms with an irradiation power of 87 Hz) were used to saturate nuclear magnetization for the protein resonances. The RF saturation pulse train was followed by a hard 90° pulse, a $T_{1\rho}$ filter with a strength of 4960 Hz (40 ms) for removing residual protein signals, and a WATERGATE sequence (*25*) for suppressing the solvent signals before data acquisitions. The proton NMR resonance range for PLA2 is −0.2 to 9.5 ppm, and 0.5−4 ppm for decylsufate. The frequency of the Gaussian pulse train was set to the off-resonance frequency at 30 ppm and the on-resonance frequency at 6.7 ppm. The STD-NMR signal results from the difference between the NMR signals with on- and off-resonance irradiation. The subtraction was carried out by a phase cycling scheme. The STD spectra were coadded and averaged from 6144 scans and an RF irradiation time of 2.1 s.

RESULTS

The mutants used for this study were designed to explore the effect of substitutions on the coupling of the active site (H48, D99, Y52, Y69, and Y73) and the interface binding (57−71 loop, L31, K53, and K56) presumably via the highly conserved H-bonding network (Figure 1). Among the mutants listed in Tables 1−4, our focus for detailed studies will be on the ones that show a significant change in the processive interfacial catalytic turnover rate (v_o) at mole fraction $X_S^* = 1$ of DMPM substrate vesicles. In most cases, the effect of single-residue substitutions in the H-bonding network (*26*−*28*) or the 57−71 loop (*10, 29*) on v_o is modest. However, certain substitutions have a significant effect on how the decylsulfate binding parameters (eq 1) are influenced by PCU (Figure 2), pH (Figures 2 and 3), and calcium concentration (Figure 4). As developed in the Appendix, these results can be interpreted in terms of a T to R allosteric change associated with the formation of $E_2^{\#}$.

Coupling of the Decylsulfate Binding to the i-Face with PCU Binding to the Active Site. Calcium binds to the catalytic site of PLA2 with a K_{Ca}^1 of 0.32 mM at pH 8.0, and the apparent K_{Ca}^1 is considerably lower if an inhibitor is bound to the active site (*30, 31*). This calcium is obligatorily required for the substrate binding and also for the chemical step (*16, 32*) mediated by H48-D99 (*16, 33*). As summarized in Table 1, the effect of 0.5 mM calcium on the decylsulfate binding to PLA2 is weak, which shows that the catalytic calcium is not required for the decylsulfate binding to the i-face. This result is consistent with the result that the affinity of decylsulfate for the active site of $E_i^{\#}$ and E* is poor with a K_1^* of >0.5 mole fraction both in the presence and in the absence of calcium (*3*).

The low affinity of decylsulfate for the active site of $E_i^{\#}$ permits study of the effect of inhibitors on the decylsulfate binding parameters (*5*). PCU with an *sn*-2-amide group is a

Table 1: Effect of Calcium (millimolar), pH, and 5 μM PCU on Decylsulfate Binding to PLA2[a]

pH	[PCU]	[Ca]	$K_1^{\#}$	$K_2^{\#}$	$K_3^{\#}$	a_1	a_2	a_3	n_1	n_2	n_3	v_o (s^{-1})
						PLA2						
8.0	0	eg	0.04	1.35		0.12	0.49		1.4	5		
	0	0.5	0.12	1.1	5.2	0.18	0.54	0.52	1.6	6	8	270
	0	20		0.38		0.05	0.75			5		
	5 μM[b]	0.5	0.07	0.5	2.5	0.10	1.02	1.15	1	3.4	3	
6.9	0	eg	0.033	0.79	2.9	0.24	0.58	0.54	1.7	8	6	
	0	0.5	0.08	0.76	3.0	0.28	0.67	0.64	1.6	7	8	
	0	20		0.25			0.73			6		
	5 μM[b]	0.5	0.047	0.43	2.47	0.27	0.72	0.52	1.2	5	5	
4.0	0	0.5	0.02	0.15	2.3	0.10	0.80	0.01	2.3	8	4	
	0	20	0.03	0.16		0.12	0.75		1.8	10		
	5 μM[b]	0.5	0.02	0.12	2	0.14	0.72	0.41	2	8	1.4	
						H48Q						
8.0	0	eg		2.6		0.02	0.56			3		
	0	0.5		1.2		0.02	0.58			4		0.0001
	5 μM[b]	0.5	<0.02	0.13		0.1	0.21		2	2		
4.0	0	eg		0.74		−0.01	0.43			3		
	0	0.5		0.24		0.04	0.57			3		
	5 μM[b]	0.5	<0.02	0.15		0.04	0.69		1	5.3		

[a] In this and other tables, the calcium concentrations and $K_i^{\#}$ values are in millimolar; eg, in 1 mM EGTA and 1 mM EDTA with no added calcium. Uncertainty in the reported fit parameters is <30%. [b] $K_i^{\#}$ values in the presence of PCU are $K_i^{\#,app}$ (eq 2).

Table 2: Effect of Calcium and pH on Decylsulfate Binding to PLA2 Mutants

mutant	pH	[Ca]	$K_1^{\#}$	$K_2^{\#}$	a_1	a_2	n_1	n_2	v_o (s^{-1})
D99A	8.0	0.5		0.35	0.02	−0.50		1	<1
		eg	0.1	0.69	−0.11	−0.39	1.5	2	
	4.0	0.5		0.08	−0.06	−0.40		3	
		eg		0.10	−0.05	−0.50		2	
H17,115N	8.0	0.5	0.4	1.2	0.18	0.56	1.6	6	300
		eg	0.4	3	0.15	0.47	1	4	
	4.0	0.5		0.35	0.03	1.0		7	
		eg	0.5	1.8	0.16	0.58	1.7	4	
proPLA	8.0	0.5	0.14	2.9	0.13	0.3	1	2	<1
		eg			0.02	0.06			
	4.0	0.5		0.4	0.03	0.27		5	
		eg		0.9	0.05	0.29		4	

Table 3: Fit Parameters for Decylsulfate Binding to (62−66 loop deleted) ΔPLA2 Mutants[a]

mutant	$K_1^{\#}$	$K_2^{\#}$	a_1	a_2	n_1	n_2	v_o (s^{-1})
ΔPLA2 at pH 8.0	0.04	0.50	0.08	2.2	1.2	6	130
ΔPLA2 at pH 4.0		0.13	0.03	0.63	1.5	6	
Δ52,73F at pH 8.0	0.15	0.65	0.18	0.75	1.5	8	75
Δ52,73F at pH 4.0	0.1	0.14	0.15	0.43	1	7	
Δ73F	0.03	0.42	0.08	1.25	1	5	130
Δ73L			0.02	0.05			7
Δ52F		0.44	0.06	1.4		6	130
Δ69K	0.12	0.74	0.2	1.0	3	9	142
Δ69F	0.06	0.6	0.07	1.2		7	34
Δ69F,53M	0.10	0.5	0.09	1.1		8	47
Δ69F,56M	0.12	0.7	0.09	0.96		6	35
Δ69F,53M	0.10	0.5	0.09	1.1		8	47
Δ31R,53M	0.12	0.7	0.07	1.4		6	42
Δ31R,56M	0.12	0.7	0.07	1.4		6	53
Δ31R,53,56M	0.13	0.63	0.07	1.3		6	24
Δ31R,69F	0.11	0.57	0.07	1.3		6	25

[a] At pH 8.0 in 0.5 mM Ca.

Table 4: Estimated Parameter Values for Decylsulfate Binding to ΔY52L[a]

pH	[PCU]	[Ca]	$K_1^{\#}$	$K_2^{\#}$	$K_3^{\#}$	$a_1 = a_2$	a_3	n_1	n_2	n_3	v_o (s^{-1})
8.0	0	0.5	0.01	0.078	5.9	0.78	−0.33	1.2	>1	0.7	11
4.0	0	0.5	0.006	0.075	3.5	0.57	−0.1	1		0.74	
8.0	15 μM[b]	0.5	0.01	0.064	5	0.42	0.1	1.4	>1	0.8	
4.0	15 μM[b]	0.5	0.01	0.057		0.22		1	>1		

[a] Uncertainty in the reported fit parameters in this table is 30%. [b] $K_i^{\#}$ values in the presence of PCU are $K_i^{\#,app}$ (eq 2).

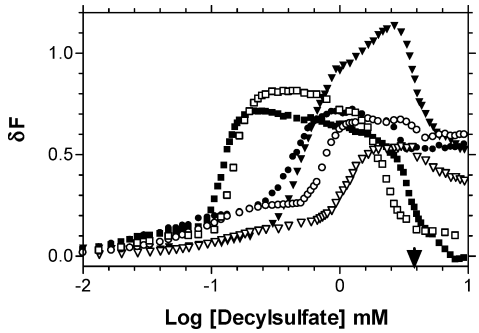

FIGURE 2: Decylsulfate concentration-dependent change in the Trp-3 fluorescence emission intensity at 333 nm (excitation at 280 nm) of 2 μM PLA2 in 0.5 mM $CaCl_2$ at pH 4.0 (squares), 6.9 (circles), and 8.0 (triangles) without (white symbols) or with (black symbols) 5 μM PCU. The fit parameters are listed in Table 1. The effect of 5 μM PCU on the fluorescence change from free enzyme is negligible. Note that in several cases the signal changes at the CMC (4.5 mM).

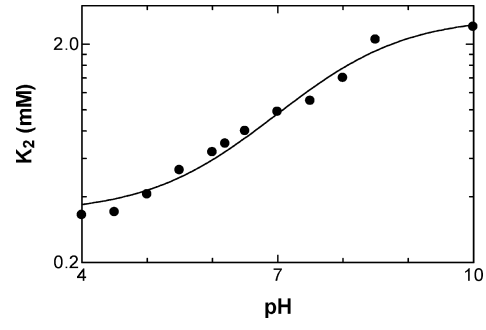

FIGURE 3: pH dependence of $K_2^{\#}$ (on the log scale) for decylsulfate binding to PLA2 in the absence of calcium. Qualitatively similar results were obtained in the presence of 0.5 mM calcium.

potent competitive inhibitor of PLA2 (*29*) with an X_I*(50) of 0.004 mole fraction (*34*) and a K_I* of 0.001 mole fraction for the E*I complex (*35*). The effect of 5 μM PCU on the decylsulfate binding curve is shown in Figure 2. Controls showed that the PCU-induced shift in the titration curve, which is prominent at the higher pH, is observed only in the presence of the catalytic calcium.

A significant result in Figure 2 is that the PCU-induced shift in the binding curve is much greater at pH 8 than at pH 4: $K_2^{\#}$ is shifted from 1.1 to 0.5 mM at pH 8 and from 0.24 to 0.15 mM at pH 4 with addition of 5 μM PCU (Table 1). Two pH effects are at work here. In the crystal structure, the δNH group of H48 is hydrogen bonded to the *sn*-2-amide NH group of PCU (*29*). It has been suggested that the affinity

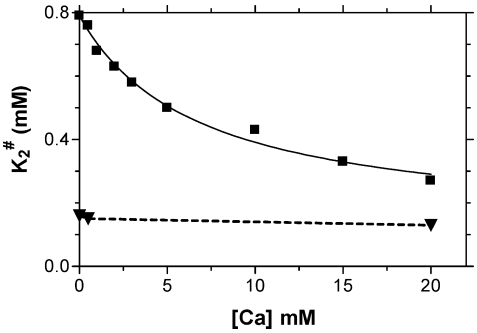

FIGURE 4: Calcium concentration dependence of $K_2^{\#}$ for the deylsulfate binding to PLA2 at pH 6.9 (■) and 4.0 (▼). The fit line for pH 6.9 results is for the apparent K_{Ca}^2 of 6.7 mM with a saturating $K_2^{\#}$ of 0.12 mM.

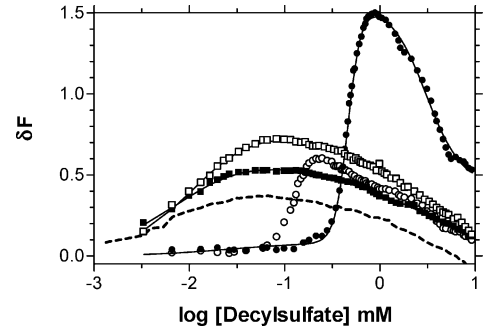

FIGURE 5: Change (normalized) in the Trp-3 emission intensity of 2 μM ΔPLA2 at pH 8 (●) or (○) 4 and of 2 μM ΔY52L at pH 8 (■) or 4 (□). The dashed line is for the titration of 2 μM ΔY52L at pH 8 in the presence of 15 μM PCU. The fit parameters for ΔPLA2 are summarized in Table 3. Assuming $a_2 = a_1$, the best fit for ΔY52L (Table 1) at pH 4 occurs if $a_2 = a_1 = 0.57$ and $a_3 = -0.096$ with $K_1^{\#} = 0.006$, $n_1 = 1.2$, $K_2^{\#} = 0.05-0.1$, $n_2 > 1$, $K_3^{\#} = 3.5$, and $n_3 = 0.74$. The best fit at pH 8 occurs if $a_2 = a_1 = 0.78$, $a_3 = -0.33$, $K_1^{\#} = 0.010$, $n_1 = 1.2$, $K_2^{\#} = 0.05-0.1$, $n_2 > 1$, $K_3^{\#} = 5.9$, and $n_3 = 0.7$.

of PCU for the active site would be higher at higher pH where the δNH group of H48 is deprotonated (*36*). This pH effect is not expected with H48Q. The results in Table 1 show that, compared to the wild-type (WT) value the apparent $K_2^{\#}$ value for H48Q changes little with pH: 0.13 mM at pH 8 versus 0.15 mM at pH 4. However, note that the apparent $K_2^{\#}$ value for H48Q in the presence of PCU is significantly lower at pH 8 compared to that for WT, suggesting a significant effect of this substitution of the catalytic H48 on the i-face interactions. Another pH effect can also be dissected. In the absence of PCU and both in the presence and in the absence of 0.5 mM calcium, the pH effect on $K_2^{\#}$ is ~8-fold for PLA2 and ~5-fold for H48Q. As discussed next, this pH effect on the formation of $E_2^{\#}$ is attributed to E71.

The Second Calcium Compensates for the Effect of High pH on $K_2^{\#}$. PLA2 binds the second calcium via a low-affinity site that includes E71, and possibly D66 and E92 (*37*). This influences the PLA2 binding to the zwitterionic interface with a K_{Ca}^2 of 5 mM at pH 8 and 2 mM at pH 6.5 (*13*). Thus, this pH effect is not seen at 50 mM calcium, and results with the E71N mutant showed that E71 with a pK_a of 6.3 (*31*) is involved in the binding of the second calcium. As shown in Figure 3, the pH-dependent increase in $K_2^{\#}$ for PLA2 has pK_a of 6.5. Also, results in Figure 4 show that $K_2^{\#}$ values for PLA2 decrease with an increase in calcium concentration, and at pH 4, $K_2^{\#}$ changes little with calcium concentration. At pH 6.9, K_{Ca}^2 is 6 mM with a limiting $K_2^{\#}$ value of 0.15 mM at the saturating calcium concentration. These results are also consistent with the effect of 20 mM calcium at pH 4, 6.9, and 8 on decylsulfate binding to PLA2 (Table 1).

In Tables 1−3, we compare the decylsulfate (pK_a < 2) binding parameters for several other mutants at pH 4 and 8. Typically, the pH effect on $K_1^{\#}$ is insignificant, and it is 3−8-fold on $K_2^{\#}$. For example, the pH effect on $K_2^{\#}$ is ~4-fold for the H17N/H115N double mutant and also for H48Q, which rules out a role for these histidines in the pH dependence of decylsulfate binding. The 5-fold pH effect on $K_2^{\#}$ for D99A also rules out a role for the D99-H48(εNH) catalytic diad. The 5-fold pH effect with pro-PLA2 with seven extra residues at the N-terminus also rules out a role for the free amino group of Ala-1 and the highly conserved structural water molecule, W1 (Figure 1).

The decylsulfate binding parameters for the mutants of ΔPLA2 are compared in Table 3. A modest effect of Asp-66, possibly involved in the binding of the second calcium, is apparent in a 4-fold pH effect on $K_2^{\#}$ for ΔPLA2 compared to the 7-fold pH effect on PLA2. Substitutions at positions 31, 53, 56, and 69 in ΔPLA2 had no additional effect on $K_2^{\#}$, although charge compensation of Lys-53 and Lys-56 in PLA2 has a modest effect on the i-face interactions with the zwitterionic interface (*3, 27, 38, 39*). Substitution of Leu-31 and Tyr-69 in ΔPLA2 had a small effect on decylsulfate binding, although both of these residues are in contact with the inhibitor in the active site (*29, 40, 41*). The decylsulfate binding parameters for the Trp substitution mutants (*20*) were also comparable to those of PLA2 with or without PCU, although a_i values from Trp at positions 6, 10, 19, 20, and 31 are noticeably different (results not shown).

The hydroxyl groups of Tyr-52 and Tyr-73 are part of the highly conserved H-bonding network (Figure 1) that is conserved in all secreted PLA2 forms (*15, 26−28*). The decylsulfate binding behaviors of the Y52 and Y73 substitution mutants of ΔPLA2 are particularly revealing. As summarized in Table 3, the Y to F substitution of one or both of these tyrosines in ΔPLA2 has at best a modest effect on any of the parameters. On the other hand, ΔY52L (Table 4) and ΔY73L (Table 3) are catalytically impaired. The Y to L substitution also has a significant effect on the Trp-3 emission peak intensities of the E form. Compared to the relative intensity of 1 for free PLA2, it is 1.5 for ΔY73L, 0.75 for ΔY52L, and 0.43 for ΔPLA2. Low a_i values for the $E_i^{\#}$ complexes of ΔY73L precluded detailed analysis. Results described next show that the Y52L substitution in ΔPLA2 has a dramatic effect on decylsulfate binding and the associated functional changes.

Anomalous Decylsulfate Binding to ΔY52L. The decylsulfate binding behavior of ΔY52L (Table 4) is significantly different compared to that of ΔPLA2 or any other mutant that we tested. The difference provides a useful insight into the coupling of the active site and i-face events. Decylsulfate binding curves of virtually all PLA2 and ΔPLA2 mutants showed three well-resolved steps with a significant effect of pH and PCU on $K_2^{\#}$. However, results in Figure 5 show that the curves for ΔPLA2 and ΔY52L are different at pH 4 and 8. Not only is the shape of the curves for ΔY52L anomalous, but the effect of pH or PCU is hardly noticeable. The decylsulfate binding to ΔY52L is fitted with two assumptions

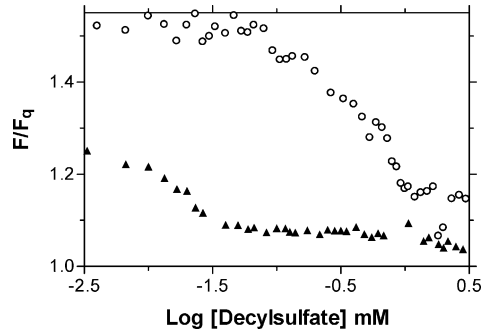

FIGURE 6: Decylsulfate concentration dependence of the relative quenching (F/F_q ratio): (○) PLA2 and (▲) ΔY52L mutant at pH 8.0 in 10 mM Tris, 10 mM NaCl, and 0.5 mM $CaCl_2$. F is the emission intensity without and F_q the emission intensity with 0.15 M succinimide.

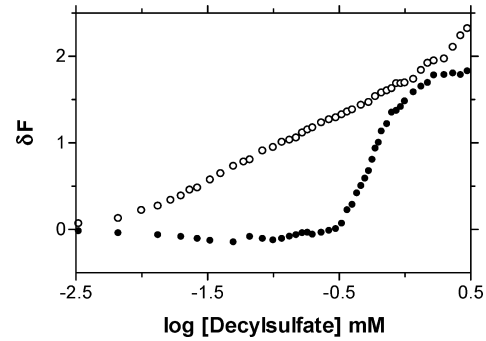

FIGURE 7: Decylsulfate concentration (log scale) dependence of the RET signal (excitation at 280 nm, emission at 450 nm) from a mixture of 1 μM TMA-DPH with 1 μM ΔPLA2 (●) or ΔY52L (○) at pH 8.0 in 10 mM Tris, 10 mM NaCl, and 0.5 mM $CaCl_2$.

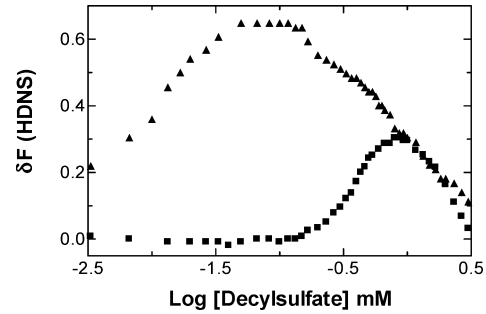

FIGURE 8: Decylsulfate concentration dependence (log scale) of the RET signal (excitation at 290 nm, emission at 490 nm) from a mixture of 1 μM HDNS and 1 μM ΔY52L (▲) or ΔPLA2 (■) at pH 8.0 in 10 mM Tris, 10 mM NaCl, and 0.5 mM $CaCl_2$.

to obtain the parameters summarized in Table 4. First, the rising phase is due to $E_1^\#$ and $E_2^\#$ formation, and the falling phase is due to $E_3^\#$. Results described below show clustering of bound decylsulfate with the formation of $E_2^\#$. As it is difficult to imagine amphiphile clustering without any Hill cooperativity, this leads to the second assumption that $E_2^\#$ is "hidden" behind $E_1^\#$ (i.e., $a_2 = a_1$), and therefore, $K_2^\#$ cannot be clearly resolved as in other cases where the two steps are well separated. This crucial assumption leaves n_2 virtually indeterminate from the fit. Apparently, the first two steps are not resolved for ΔY52L, as expected if there is no conformational change in the formation of $E_2^\#$. Furthermore, the Trp-3 signal at 333 nm at the peak in the decylsulfate titration curve for ΔY52L ($F = 45$ at pH 8 and 0.5 mM calcium) is in fact higher than the peak [$F = 34$ (cf. Figure 5)] for ΔPLA2. At the same time, the basal signal (in the absence of decylsulfate) is higher for ΔY52L than for ΔPLA2 ($F_0 = 27.3$ vs 13.6) as if ΔY52L even without decylsulfate present is closer to the conformation (R) with the larger signal.

Clustering of Decylsulfate on ΔY52L. The Hill numbers for most of the mutants in Tables 1−3 show cooperative clustering of many decylsulfate molecules around Trp-3 on the i-face. Since n_i is expected to be smaller than the binding stoichiometry, N_i (eq 1), in most mutants a total of at least 2, 10, and 20 decylsulfate molecules are bound to $E_1^\#$, $E_2^\#$, and $E_3^\#$, respectively. This is consistent with the result that the quencher accessibility of Trp-3 decreases for the higher $E_i^\#$ complexes (*2, 3*) and E* (*42*). However, in spite of the apparent loss of Hill cooperativity, significant clustering occurs in ΔY52L measured at sufficiently low enzyme and high decylsulfate ratios. As shown in Figure 6, Trp-3 is less quenched by succinimide in ΔY52L than in PLA2. Also, for PLA2, an abrupt decrease occurs at >0.5 mM decylsulfate, whereas for ΔY52L, the abrupt decrease is nearly complete at 0.1 mM decylsulfate. This difference is consistent with the estimated $K_2^\#$ values. The kinetics of covalent modification of ΔY52L with *N*-bromosuccinimide is significantly slower at 0.1 mM decylsulfate (results not shown) which is expected if decylsulfate molecules clustered around Trp-3 shield access to the reagent (*3, 20*).

Clustering of several decylsulfate molecules on ΔY52L is also affirmed by the behavior of the RET probes partitioned in the $E_i^\#$ complexes (*2, 17, 43, 44*). As shown in Figure 7, at low decylsulfate concentrations the shape of the titration curve with ΔY52L is noticeably different compared to that with ΔPLA2. The signal from ΔPLA2 and TMA-DPH is modestly quenched with the formation of $E_1^\#$ at <0.4 mM decylsulfate and then increases sharply with the formation of $E_2^\#$. In comparison, the signal intensity from ΔY52L and TMA-DPH is larger and increases at low decylsulfate concentrations but not abruptly. Also, the results in Figure 8 show that the RET signal from the HDNS acceptor in the presence of ΔY52L peaks at 0.1 mM decylsulfate, and thereafter, the intensity decreases with $E_3^\#$ formation well below the CMC. On the other hand, with ΔPLA2 the magnitude of the RET signal from HDNS increases abruptly at higher decylsulfate concentrations where $E_2^\#$ forms. The relative differences between the behaviors of TMA-DPH and HDNS acceptors suggest differences in their RET characteristics which cannot be readily modeled because such contributions cannot be independently resolved (*2, 43*).

The STD-NMR spectra describe the epitopes of decylsulfate protons that interact with the protein and other decylsulfate molecules in the $E_i^\#$ complexes of PLA2 (*3*). As shown in Figure 9, at 0.2 mM decylsulfate (spectrum a), the STD signals of the protons at C_3−C_{10} of decylsulfate bound to ΔPLA2 (in panel A) are noticeably less pronounced than those from ΔY52L (in panel B) under otherwise identical conditions. Here our focus is on the observed differences for ΔPLA2 versus ΔY52L under otherwise identical conditions. The epitope from 0.2 mM decylsulfate and ΔPLA2 is weak, which is expected for the $E_1^\#$ complex with two or three decylsulfate molecules bound. On the other hand, the STD spectra (b) from 1.2 mM decylsulfate and ΔPLA2 or from 0.2 or 1.2 mM decylsulfate with ΔY52L are comparable as expected for the epitope of $E_2^\#$ where 5−10 decylsulfate molecules are likely to be contiguously clustered. Also, the

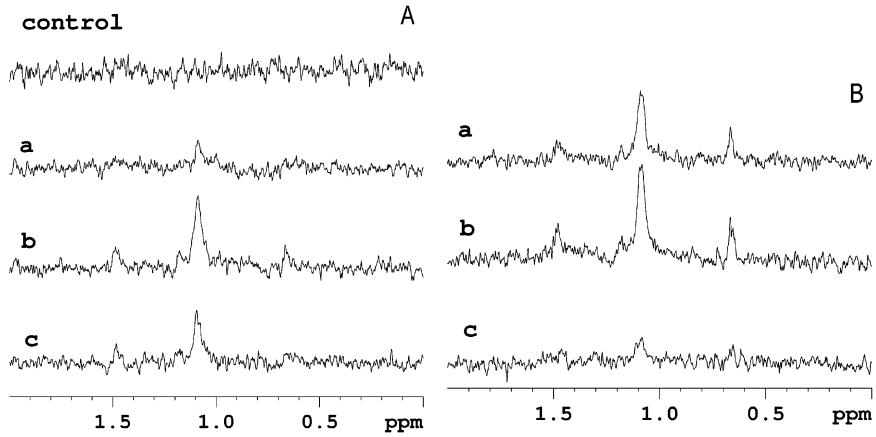

FIGURE 9: STD-NMR spectra of (bottom in panel A) 0.2 mM decylsulfate alone or 0.2 mM decylsulfate in the presence of 0.5 μM ΔPLA2 (A) or ΔY52L (B). Only the 0.5−1.5 ppm region is shown. The control in panel B with 0.2 mM decylsulfate alone showed no STD signal. Spectra in the presence of 0.5 μM enzyme (a), 0.2 or 1.2 mM decylsulfate (b), or 0.2 mM decylsulfate and 1.5 μM PCU (c). These spectra were recorded with 6000 pulses with a duration of 50 μs and a saturation time of 1 s at 15 °C in 20 mM bicarbonate buffer in D_2O (99%) at pH 7.5.

Table 5: Interfacial Kinetic Parameters for ΔPLA2 and ΔY52L at 0.5 mM Calcium and pH 8

substrate	parameter	PLA2	ΔPLA2	ΔY52L
DMPM (0.4 mM) vesicles	v_o (s^{-1})	270	130	11
	MJ33 X_I*(50) mole fraction	0.0032	0.006	0.009
	PCU X_I*(50) mole fraction	0.0016	0.004	0.004
DC_7PC (5.2 mM) micelles in 4 M NaCl	V_M^{app} (s^{-1})	660	600	34
	K_M^{app} (mM)	0.2	0.1	0.05
	MJ33 X_I*(50) mole fraction	0.012	0.006	0.04
	PCU X_I*(50) mole fraction	0.003	0.0032	0.004
DC_7PC (5.2 mM) micelles in 1 mM NaCl	V_M^{app} (s^{-1})	16	83	2.5
	K_M^{app} (mM)	2.3	1.2	2.5
	MJ33 X_I*(50) mole fraction	0.02	0.003	0.11
	PCU X_I*(50) mole fraction	0.005	0.002	0.004

epitope for 0.2 mM decylsulfate and ΔPLA2 changes in the presence of 1.5 μM PCU (spectrum c in panel A). This change resembles the change from $E_1^{\#}$ to $E_2^{\#}$ (a vs b) which suggests clustering of more decylsulfate molecules on ΔPLA2 in the presence of PCU. On the other hand, the epitope in 0.2 mM decylsulfate and ΔY52L becomes noticeably weaker in the presence of 1.5 μM PCU (b vs c in panel B), suggesting a perturbed coupling of the i-face and active site events. Together, results in Figures 5−9 show that at lower concentrations decylsulfate molecules are clustered on ΔY52L and that this is not influenced by pH. Also, comparable effects of decylsulfate in all of these experiments are observed in the presence or absence of calcium. Such controls ruled out the possibility that the anomalous behavior of ΔY52L is due to enhanced binding of decylsufate to the active site.

ΔY52L Is Catalytically Impaired at the Interface. The kinetic results in Table 5 show that the processive interfacial turnover rate on DMPM vesicles, v_o, is 270 s^{-1} for PLA2 compared to 11 s^{-1} for ΔY52L and 130 s^{-1} for ΔPLA2. In this assay, both ΔY52L and ΔPLA2 are 50% inhibited by PCU with an X_I*(50) of 0.004 mole fraction. For MJ33, X_I*(50) is 0.009 mole fraction for ΔY52L, compared to 0.006 mole fraction for ΔPLA2 and 0.0032 mole fraction for PLA2. As also summarized in Table 5, the difference in the inhibitory effect of PCU versus MJ33 is more significant on DC_7PC micelles where the V_M^{app} increase at the high salt concentration is attributed to the k_{cat}* activation by the interfacial anionic charge induced by a preferential partitioning of chloride versus sodium in the substrate micelles (*7*). Also, the salt effect on K_M^{app} for ΔPLA2 is 12-fold compared to 50-fold for ΔY52L. This effect is likely to be dominated by the salt effect in the binding of enzyme to the substrate interface (*7*).

The X_I*(50) value for the inhibition of ΔY52L on DC_7PC micelles in 1 mM NaCl by *sn*-2-tetrahedral mimic MJ33 is 35-fold larger than that for ΔPLA2 compared to the 7-fold difference in 4 M NaCl and 1.5-fold on DMPM vesicles. On the other hand, for the *sn*-2-amide substrate mimic PCU, the observed range for X_I*(50) is only 2-fold for the three enzymes in all three assays. These results show that the Y52L substitution lowers the affinity for the tetrahedral mimic MJ33 and that the effect appears to depend on the interface. These results suggest that the Y52L substitution in ΔPLA2 lowers the affinity for the *sn*-2-tetrahedral intermediate along the reaction path (*16, 32, 45*), without a significant change in the affinity for the substrate. This could account for a lower turnover rate due to the partitioning of the interfacial Michaelis complex E*S of ΔY52L away from the transition state.

DISCUSSION

Results with the premicellar complexes of PLA2 show that some of the changes associated with the formation of $E_2^{\#}$ are parallel to those associated with the interface-activated E* state. Also, for most of the mutants of PLA2, the apparent $K_2^{\#}$ values decrease at lower pH, at high calcium concentrations, and in the presence of PCU where the lower-limit $K_2^{\#}$ values are ~0.12 mM compared to a value of 1.35 mM at

pH 8. However, the $K_2^{\#}$ for ΔY52L remains 0.1 mM without a noticeable effect of pH, high calcium concentration, or the presence of PCU. We suggest that $K_2^{\#}$ and the underlying structural change are a proxy for the K_S* allosteric change observed at the interface (*6, 7*). As developed in the Appendix, we adopt the concept of the T (inactive) to R (active) allosteric transition to suggest that interfacial activation involves such coupling between the i-face on the surface and the catalytic active site in the interior of PLA2 (*4, 16, 21, 24*).

The T to R Transition for Interfacial Allostery. In analogy with the classical model found in textbooks for the concerted allosteric transition in hemoglobin, we assume that PLA2 can exist in an inactive T or active R conformation. Operationally, for the interfacial allostery, the single subunit of PLA2 in E or E* corresponds to the T or R form, respectively. The T form binds poorly both to the interface and at the active site. Binding to the interface promotes a transition to the R conformation which binds substrate or inhibitor well at the active site. Conversely, binding at the active site also promotes the R conformation which binds the interface well. Thus, E in the aqueous phase at high pH would be mostly in the inactive T form, while E*(S) at the interface would be mostly in the R form. Currently available methods cannot structurally distinguish the T and R forms of the E* form of PLA2.

Results with the premicellar complexes suggest that the T to R transition may develop in stages. Also, a difference in the effects of calcium, pH, and PCU and the effects of the H48Q substitution in WT or of the Y52L substitution in ΔPLA2 shows a structural role analogous to that for the T to R transition. In this interpretation, besides a modest effect on $K_1^{\#,app}$ seen in the E to $E_1^{\#}$ step, at least some of the features of the T to R transition are significant in the $E_1^{\#}$ to $E_2^{\#}$ step (*5*). We interpret the decrease in the apparent $K_2^{\#}$, i.e., an increase in the affinity of decylsulfate for the i-face, as a proxy for the underlying structural change that is analogous to the T to R transition in the K_S* allosteric activation. The lowest values of $K_2^{\#}$ (ca. 0.1 mM) are indicative of the R conformation that is induced not only by active site binding or i-face binding but also by low pH or high calcium, where $E_2^{\#}$ would be R-like with enhanced affinity for the substrate.

Apart from the T to R transition, there is an additional pH effect due to protonation or deprotonation of H48 in the active site. While low pH would induce the R state with strong active site binding to WT, this pH effect is not seen with H48Q where the apparent $K_2^{\#}$ with PCU present is virtually the same at pH 4 and 8. This effect complements but is different from the effect of protonation of H48 that is also expected to destabilize the active site binding with a possible role in the reaction mechanism (*32*). ΔY52L with or without PCU appears to be frozen in the R state. It binds to the interface well, and it also binds the *sn*-2-amide mimic PCU well to the active site but not the *sn*-2-tetrahedral mimic MJ33 (Table 5). These results implicate a role of the interface in the chemical step because the difference is much larger at the zwitterionic interface than at the anionic interface. Thus, in addition to, or as a consequence of, the impaired R to T transition, the Y52L substitution may hinder the approach of E* toward the transition state.

Cooperativity of the Amphiphile Binding to the i-Face. Formation of $E_1^{\#}$ is a discrete step that is only modestly affected under most conditions that we have examined. For example, in the absence of calcium at pH 6.9 for PLA2, $K_1^{\#}$ is 40 μM with a Hill number (n_1) of 1.7. More than one and possibly two or three decylsulfate molecules would be bound, but none to the active site. This is followed by cooperative and contiguous binding of six to eight additional amphiphiles in $E_2^{\#}$. Binding of additional amphiphiles around a core or nucleus in the $E_1^{\#}$ to $E_2^{\#}$ step could contribute to the cooperativity where individual amphiphiles stabilize the binding of more just through neighbor interactions.

The possibility that formation of $E_1^{\#}$ involves some conformational change that could promote further amphiphile binding to form $E_2^{\#}$ cannot be excluded. In contrast to $K_2^{\#}$, $K_1^{\#}$ is not significantly influenced by PCU, pH, or high calcium concentrations (Table 1). Thus, formation of $E_1^{\#}$ does not appear to involve a step on the way from the T to R transition. On the basis of the pH effect and the effect of the second calcium at high pH, both associated with E71, we suggest that the 57−72 loop plays a critical role in the formation of $E_2^{\#}$ which significantly enhances the Trp-3 emission signal and also has a higher affinity for PCU.

Allosteric Effect of Cooperative Binding. Thermodynamic microscopic reversibility requires that inhibitor−enzyme binding be activated by the interface by the same factor as the enzyme−interface binding is activated by inhibitor binding to the active site of PLA2 (*5*). Thus, the lower apparent $K_2^{\#}$ ($K_2^{\#,app}$) value in the presence of PCU qualitatively shows that this relationship holds for the $E_2^{\#}$ complexes. For most mutants, the coupling observed during the formation of $E_2^{\#}$ is influenced by pH and by the binding of the second calcium or PCU. These effects are impaired in ΔY52L. A quantitative interpretation of the $K_2^{\#,app}$ value at low PCU concentrations is unlikely to be corrupted by PCU binding to the i-face. The magnitude of the change provides useful insights. The 2-fold lower $K_2^{\#,app}$ in the presence of 5 μM PCU implies a 2-fold change on average for each of the n_2 amphiphiles involved in the cooperative complex. Thus, if 6 amphiphiles are involved in the $E_i^{\#}$ and $E_i^{\#}$I complexes, and if binding of PCU causes a 2-fold change in $K_i^{\#}$, then formation of $E_i^{\#}$ would cause a 2^n-fold change in the binding of PCU to the active site. Thus, while a 2-fold effect on the estimated $K_2^{\#}$ may appear to be fairly modest, it translates into a much larger effect on active site binding. Furthermore, it is also consistent with the K_S* activation factor of 10−100 for PLA2 depending on the interface and the ligand or substrate (*4, 6, 21, 24, 35, 46*), and also with the pH effect on $K_i^{\#}$ as interpreted in the Appendix.

ΔY52L Remains in the R State and Cannot Undergo the Allosteric Change. Results in Table 4 show that the anomalous decylsulfate binding to ΔY52L is considerably tighter with apparently low Hill numbers. Also, results in Figures 6−9 show that the decylsulfate molecules bound to ΔY52L are clustered. The first two steps for the decylsulfate binding to ΔY52L are not resolved, and the estimated limiting $K_2^{\#}$ value remains 0.1 mM without a significant effect of PCU, high pH, or calcium concentration. These results suggest that ΔY52L remains in the R state. The change in the turnover rate is interpreted below with the assumption that the chemical step for ΔY52L remains rate-limiting as is the case for WT (*47*).

Structural Basis for Rate Impairment of ΔY52L. Y52L is in a conformation with strong interfacial binding (both as

$E_2^{\#}$ and as E*), which suggests that the i-face is in the K_S*-activated R state at the higher pH, which is also optimal for catalysis. However, kinetic results in Table 5 show that the turnover rate of ΔY52L at pH 8 is impaired both on the zwitterionic and on the anionic interface where the affinities of PCU relative to that of the substrate are similar for the turnover by ΔY52L, ΔPLA2, and PLA2. Therefore, on the basis of the results with MJ33, we suggest that the Y52L substitution changes the chemical step such that the interfacial Michaelis complex E*S is partitioned away from the tetrahedral intermediate or the transition state (*7, 21, 24, 38*).

To recapitulate, results with H48Q and ΔY52L suggest that these substitutions could mediate their effects on $K_2^{\#}$ via the highly conserved $H_{48}DXCY_{52}$ sequence. Changes in the helical segment could also involve catalytic site residue D49 and the H48-D99 diad (*32*). The C51−C98 disulfide bridge is also conserved in all calcium-dependent secreted PLA2 (*16*). Another structural feature of interest is the 57−72 loop. It is normally disordered (*48, 18*), and it becomes noticeably more ordered in the complex with inhibitor (*29, 49*), in the anion-assisted dimer structure (*50*) where the cationic charges around the i-face are compensated, and in the mutant with quadruple K to M substitutions at positions 53, 56, 120, and 121 (*37*). We suggest that the T to R transition may involve changes in the 56−71 loop on the surface, also implicated by the regulatory role of bile salts (*17*), to couple the i-face interactions with the active site events via the $H_{48}DXCY_{52}$ sequence as a part of the rigid 42−56 helix.

APPENDIX

To give a flair for what a concerted R to T allosteric mechanism for an interfacial enzyme would entail, we can consider the simplest version with two premicellar complexes and two conformations where only the R state binds at the active site, while the T state is totally inactive. In the absence of amphiphile, the equilibrium is toward the inactive T state with an equilibrium constant K_0. The results indicate that presence of PCU (I) has only a marginal influence on $K_1^{\#}$. This suggests that the R state and T state form the $E_1^{\#}$ complex with the same propensity given by $K_1^{\#}$. Assuming that only the R state forms $E_2^{\#}$ with equilibrium constant $K_2^{\#,R}$, and only the R state binds I with dissociation constant K_I^R, the binding scheme for the R and T states will be.

Scheme 3

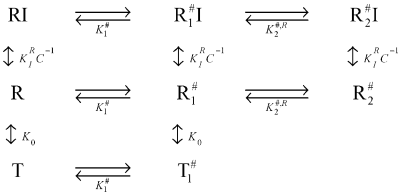

The factor $C^{-1} = 1 + K_{Ca}/[Ca]$ accounts for the binding and influence of the catalytic calcium (*5*) at concentration [Ca]. This calcium has little or no effect on the R−T equilibrium or on the i-face binding. Scheme 3 gives the apparent dissociation constant of I from the active site in the presence of amphiphile (decylsulfate) at concentration *A*

$$K_I^{app}(A) \approx \frac{K_I^R}{C}\left[1 + \frac{K_0}{1 + (A/K_2^{\#,R})^{n_2}}\right] \quad (4)$$

where the approximation holds in the limits $A \gg K_1^{\#}$ and $A \ll K_1^{\#} < K_2^{\#}$. The apparent dissociation constant for the $E_2^{\#}$ complex in the presence of inhibitor (PCU) at concentration *I* is

$$K_2^{\#,app}(I) = K_2^{\#,R}\left(1 + \frac{K_0}{1 + CI/K_I^R}\right)^{1/n_2} \quad (5)$$

Equation 5 allows us to identify at least the qualitative trends of the activation effects in Table 1. The effect of adding 5 μM PCU in the presence of 0.5 mM Ca (i.e., $C = 0.59$) can be expressed as

$$\left[\frac{K_2^{\#,app}(I=0)}{K_2^{\#,app}(I=5)}\right]^{n_2} = \frac{1 + K_0}{1 + K_0/(1 + 0.59 \times 5/K_I^R)} \quad (6)$$

Thus, for PLA2 at pH 6.9, $K_2^{\#,app}$ changes from 0.76 to 0.43 mM upon addition of PCU. Inserting the average n_2 of 6 and assuming $K_0 \gg 1 + CI/K_I^R$ gives a K_I^R of 0.1 μM; this would correspond to the maximum active site affinity at full activation. In the absence of *A*, eq 4 gives $K_I^{app}C = K_I^R(1 + K_0)$, which in the preceding paper was estimated as $K_I > 50$ μM. Thus, a K_0 of >500 is expected. Furthermore, the limiting value for $K_2^{\#,app}$ of 0.1−0.13 mM which appears for various mutants, at high PCU concentrations, at low pH, and/or at high calcium concentrations would correspond to $K_2^{\#,R}$. Thus, K_0 could be estimated from eq 5 as $K_0 = [K_2^{\#,app}(I = 0)/0.13]^{n_2} - 1$; for PLA2 at pH 6.9, this gives $K_0 \sim 10^4-10^5$.

At pH 4, the equilibrium for the free enzyme is pushed more toward the active R state and K_0 is no longer ≫1, making the corresponding quantitation of K_I^R impossible. In the absence of I, $K_2^{\#,R}$ increases by a factor 1.4 for PLA2 when the pH increases from 6.9 to 8. If it is assumed that the pH effect in eq 5 resides only in R−T equilibrium constant K_0 and not in $K_2^{\#,R}$, K_0 would be a factor $1.4^{n_2} \approx 9$ larger at pH 8 than at pH 6.9; in other words, the increased pH pushes the R−T equilibrium even more toward T. For the ΔY52L mutant (Table 4), $K_2^{\#,app}$ remains around 0.07 mM, independent of pH or the presence of PCU. In terms of eq 5, this implies $K_2^{\#,R} = 0.07$ mM and that $K_0 < 1$; thus, the equilibrium is pushed toward R. In this limit, the binding to the active site as determined by K_I^R is indeterminate from the data and could also be influenced by the mutation. Alternatively, when the coupling is destroyed, the allosteric scheme is disrupted and the ΔY52L mutant could have its i-face in the R conformation while the active site remains in something resembling the T conformation. However, the strong binding of PCU to E* (Table 5) suggests also that the active site of ΔY52L remains in the R conformation.

Although the numbers discussed above should be considered mostly as order-of-magnitude estimates, they show that the major effects and trends are consistent with the simplest possible concerted allosteric model as given by Scheme 3. The results of the previous paper suggest that PCU binding to the i-face can achieve partial activation. However, Scheme 3 does not account for the complication from PCU binding at the i-face, differences in n_2 values, and possible partial conformation changes.

REFERENCES

1. Yu, B. Z., Apitz-Castro, R., Tsai, M. D., and Jain, M. K. (2003) Interaction of monodisperse anionic amphiphiles with the i-face of secreted phospholipase A2. *Biochemistry 42*, 6293–6301.

2. Berg, O. G., Yu, B. Z., Chang, C., Koehler, K. A., and Jain, M. K. (2004) Cooperative binding of monodisperse anionic amphiphiles to the i-face: Phospholipase A2-paradigm for interfacial binding. *Biochemistry 43*, 7999–8013.
3. Bai, S., Jain, M. K., and Berg, O. G. (2008) Contiguous binding of decylsulfate on the interface binding surface of pancreatic phospholipase A2. *Biochemistry 47*, 2899–2907.
4. Jain, M. K., and Berg, O. G. (2006) Coupling of the i-face and the active site of phospholipase A_2 for interfacial activation. *Curr. Opin. Chem. Biol. 10*, 473–479.
5. Berg, O. G., Yu, B. Z., and Jain, M. K. (2009) Thermodynamic reciprocity of the inhibitor binding to the active site and the interface recognition region of IB phospholipase A2. *Biochemistry 48*, 3209–3218.
6. Jain, M. K., Yu, B. Z., and Berg, O. G. (1993) Relationship of interfacial equilibria to interfacial activation of phospholipase A2. *Biochemistry 32*, 11319–11329. [Erratum: (1994) *Biochemistry 33*, 8618].
7. Berg, O. G., Rogers, J., Yu, B. Z., Yao, J., Romsted, L. S., and Jain, M. K. (1997) Thermodynamic and kinetic basis of interfacial activation: Resolution of binding and allosteric effects on pancreatic phospholipase A2 at zwitterionic interfaces. *Biochemistry 36*, 14512–14530.
8. Lugtigheid, R. B., Otten-Kuipers, M. A., Verheij, H. M., and De Haas, G. H. (1993) Arginine 53 is involved in head-group specificity of the active site of porcine pancreatic phospholipase A2. *Eur. J. Biochem. 213*, 517–522.
9. Janssen, M. J., Verheij, H. M., Slotboom, A. J., and Egmond, M. R. (1999) Engineering the disulphide bond patterns of secretory phospholipases A2 into porcine pancreatic isozyme. The effects on folding, stability and enzymatic properties. *Eur. J. Biochem. 261*, 197–207.
10. Kuipers, O. P., Dekker, N., Verheij, H. M., and de Haas, G. H. (1990) Activities of native and tyrosine-69 mutant phospholipases A2 on phospholipid analogues. A reevaluation of the minimal substrate requirements. *Biochemistry 29*, 6094–6102.
11. Kuipers, O. P., Kerver, J., van Meersbergen, J., Vis, R., Dijkman, R., Verheij, H. M., and de Haas, G. H. (1990) Influence of size and polarity of residue 31 in porcine pancreatic phospholipase A2 on catalytic properties. *Protein Eng. 3*, 599–603.
12. Kuipers, O. P., Vincent, M., Brochon, J. C., Verheij, H. M., de Haas, G. H., and Gallay, J. (1991) Insight into the conformational dynamics of specific regions of porcine pancreatic phospholipase A2 from a time-resolved fluorescence study of a genetically inserted single tryptophan residue. *Biochemistry 30*, 8771–8785.
13. van den Bergh, C. J., Bekkers, A. C., Verheij, H. M., and de Haas, G. H. (1989) Glutamic acid 71 and aspartic acid 66 control the binding of the second calcium ion in porcine pancreatic phospholipase A2. *Eur. J. Biochem. 182*, 307–313.
14. Beiboer, S. H., Franken, P. A., Cox, R. C., and Verheij, H. M. (1995) An extended binding pocket determines the polar head group specificity of porcine pancreatic phospholipase A2. *Eur. J. Biochem. 231*, 747–753.
15. Kuipers, O. G., Frankan, P. A., Hendricks, R., Verheij, H. M., and De Haas, G. H. (1990) Function of the fully conserved residues Asp-99, Tyr-52 and Tyr-73 in phospholipase A2. *Protein Eng. 4*, 199–204.
16. Verheij, H. M., Slotboom, A. J., and de Haas, G. H. (1981) Structure and function of phospholipase A2. *Rev. Physiol. Biochem. Pharmacol. 91*, 91–203.
17. Yu, B. Z., Apitz-Castro, R., Jain, M. K., and Berg, O. G. (2007) Role of the 57−72 loop in specific interaction of bile salts with pancreatic IB phospholipase A2: Regulation of fat and cholesterol homeostasis. *Biochim. Biophys. Acta 1768*, 2478–2490.
18. Yuan, C., and Tsai, M. (1999) Pancreatic phospholipase A_2: New views on old issues. *Biochim. Biophys. Acta 1441*, 215–222.
19. Ramirez, F., and Jain, M. K. (1991) Phospholipase A2 at the bilayer interface. *Proteins: Struct., Funct., Genet. 9*, 229–239.
20. Tsai, Y., Yu, B.-Z., Wang, Y., Chen, J. W., and Jain, M. K. (2006) Desolvation map of the i-face of phospholipase A2. *Biochim. Biophys. Acta 1758*, 653–665.
21. Berg, O. G., Gelb, M. H., Tsai, M. D., and Jain, M. K. (2001) Interfacial enzymology: The secreted phospholipase A2-paradigm. *Chem. Rev. 101*, 2613–2654.
22. Jain, M. K., Rogers, J., Jahagirdar, D. V., Marecek, J. F., and Ramirez, F. (1986) Kinetics of interfacial catalysis by phospholipase A2 in intravesicle scooting mode, and heterofusion of anionic and zwitterionic vesicles. *Biochim. Biophys. Acta 860*, 435–447.
23. Berg, O. G., Yu, B. Z., Rogers, J., and Jain, M. K. (1991) Interfacial catalysis by phospholipase A2: Determination of the interfacial kinetic rate constants. *Biochemistry 30*, 7283–7297.
24. Berg, O. G., and Jain, M. K. (2002) *Interfacial Enzyme Kinetics*, Wiley, London.
25. Piotto, M., Sanudek, V., and Sklenar, V. (1992) *J. Biomol. NMR 2*, 661–664.
26. Dupureur, C. M., Yu, B. Z., Jain, M. K., Noel, J. P., Deng, T., Li, Y., Byeon, I. J., and Tsai, M. D. (1992) Phospholipase A2 engineering. Structural and functional roles of highly conserved active site residues tyrosine-52 and tyrosine-73. *Biochemistry 31*, 6402–6413.
27. Yu, B. Z., Rogers, J., Tsai, M. D., Pidgeon, C., and Jain, M. K. (1999) Contributions of residues of pancreatic phospholipase A2 to interfacial binding, catalysis, and activation. *Biochemistry 38*, 4875–4884.
28. Thunnissen, M. M., Franken, P. A., De Haas, G. H., Drenth, J., Kalk, K. H., Verheij, H. M., and Dikstra, W. (1992) Site-directed mutagenesis of two porcine pancreatic PLA2 mutants: Y52F and Y73F. *Protein Eng. 5*, 597–603.
29. Thunnissen, M. M., Ab, E., Kalk, K. H., Drenth, J., Dijkstra, B. W., Kuipers, O. P., Dijkman, R., de Haas, G. H., and Verheij, H. M. (1990) X-ray structure of phospholipase A2 complexed with a substrate-derived inhibitor. *Nature 347*, 689–691.
30. Yu, B. Z., Berg, O. G., and Jain, M. K. (1993) The divalent cation is obligatory for the binding of ligands to the catalytic site of secreted phospholipase A2. *Biochemistry 32*, 6485–6492.
31. Donne-Op den Kelder, G. M., De Haas, G. H., and Egmond, M. R. (1983) Localization of the second calcium ion binding site in porcine and equaine phospholipase A2. *Biochemistry 22*, 2470–2478.
32. Yu, B. Z., Rogers, J., Nicol, G. R., Theopold, K. H., Seshadri, K., Vishweshwara, S., and Jain, M. K. (1998) Catalytic significance of the specificity of divalent cations as K_S* and k_{cat}* cofactors for secreted phospholipase A2. *Biochemistry 37*, 12576–12587.
33. Verheij, H. M., Volwerk, J. J., Jansen, E. H., Puyk, W. C., Dijkstra, B. W., Drenth, J., and de Haas, G. H. (1980) Methylation of histidine-48 in pancreatic phospholipase A2. Role of histidine and calcium ion in the catalytic mechanism. *Biochemistry 19*, 743–750.
34. de Haas, G. H., Dijkman, R., van Oort, M. G., and Verger, R. (1990) Competitive inhibition of lipolytic enzymes. III. Some acylamino analogues of phospholipids are potent competitive inhibitors of porcine pancreatic phospholipase A2. *Biochim. Biophys. Acta 1043*, 75–82.
35. Jain, M. K., Tao, W. J., Rogers, J., Arenson, C., Eibl, H., and Yu, B. Z. (1991) Active-site-directed specific competitive inhibitors of phospholipase A2: Novel transition-state analogues. *Biochemistry 30*, 10256–10268.
36. Yu, L., and Dennis, E. A. (1991) Critical role of a hydrogen bond in the interaction of a phospholipase A2 with transition state and substrate analog. *Proc. Natl. Acad. Sci. U.S.A. 88*, 9325–9329.
37. Sekar, K., Yogavel, M., Kanaujia, S. P., Sharma, A., Velmurugan, D., Poi, M. J., Dauter, Z., and Tsai, M. D. (2006) Suggestive evidence for the involvement of the second calcium and surface loop in interfacial binding: monoclinic and trigonal crystal structures of a quadruple mutant of phospholipase A2. *Acta Crystallogr. D62*, 717–724.
38. Yu, B. Z., Poi, M. J., Ramagopal, U. A., Jain, R., Ramakumar, S., Berg, O. G., Tsai, M. D., Sekar, K., and Jain, M. K. (2000) Structural basis of the anionic interface preference and k_{cat}* activation of pancreatic phospholipase A2. *Biochemistry 39*, 12312–12323.
39. Rogers, J., Yu, B. Z., Tsai, M. D., Berg, O. G., and Jain, M. K. (1998) Cationic residues 53 and 56 control the anion-induced interfacial k_{cat}* activation of pancreatic phospholipase A2. *Biochemistry 37*, 9549–9556.
40. Scott, D. L., and Sigler, P. B. (1994) Structure and catalytic mechanism of secretory phospholipases A2. *Adv. Protein Chem. 45*, 53–88.
41. Sekar, K., Kumar, A., Liu, X., Tsai, M. D., Gelb, M. H., and Sundaralingam, M. (1998) Structure of the complex of bovine pancreatic phospholipase A2 with a transition-state analogue. *Acta Crystallogr. D54*, 334–341.
42. Jain, M. K., and Maliwal, B. P. (1993) Spectroscopic properties of the states of pig pancreatic phospholipase A2 at interfaces and their possible molecular origin. *Biochemistry 32*, 11838–11846. [Erratum: (1994) *Biochemistry 33*, 8618].

43. Berg, O. G., Yu, B. Z., Apitz-Castro, R. J., and Jain, M. K. (2004) Phosphatidylinositol-specific phospholipase C forms different complexes with monodisperse and micellar phosphatidylcholine. *Biochemistry 43*, 2080–2090.
44. Yu, B. Z., Polenova, T. E., Jain, M. K., and Berg, O. G. (2005) Premicellar complexes of sphingomyelinase mediate enzyme exchange for the stationary phase turnover. *Biochim. Biophys. Acta 1712*, 137–151.
45. Scott, D. L., White, S. P., Otwinowski, Z., Yuan, W., Gelb, M. H., and Sigler, P. B. (1990) Interfacial catalysis: The mechanism of phospholipase A2. *Science 250*, 1541–1546.
46. Jain, M. K., Yuan, W., and Gelb, M. H. (1989) Competitive inhibition of phospholipase A2 in vesicles. *Biochemistry 28*, 4135–4139.
47. Jain, M. K., Yu, B. Z., Rogers, J., Gelb, M. H., Tsai, M. D., Hendrickson, E. K., and Hendrickson, H. S. (1992) Interfacial catalysis by phospholipase A2: The rate-limiting step for enzymatic turnover. *Biochemistry 31*, 7841–7847.
48. Yuan, C., Byeon, I.-J. L., Li, Y., and Tsai, M.-D. (1999) Structural analysis of phospholipase A_2 from functional perspective. 1. Functionally relevent solution structure and roles of the hydrogen-bonding network. *Biochemistry 38*, 2909–2918.
49. Sekar, K., Eswaramoorthy, S., Jain, M. K., and Sundaralingam, M. (1997) Crystal structure of the complex of bovine pancreatic phospholipase A2 with the inhibitor 1-hexadecyl-3-(trifluoroethyl)-sn-glycero-2-phosphomethanol. *Biochemistry 36*, 14186–14191.
50. Pan, Y. H., Epstein, T. M., Jain, M. K., and Bahnson, B. J. (2001) Five coplanar anion binding sites on one face of phospholipase A2: Relationship to interface binding. *Biochemistry 40*, 609–617.

BI801245S